HHS Public Access

Author manuscript

Mol Cell. Author manuscript; available in PMC 2015 August 05.

Published in final edited form as:

Mol Cell. 2005 October 28; 20(2): 325–333. doi:10.1016/j.molcel.2005.09.001.

Structural Basis for Inhibition of the Insulin Receptor by the Adaptor Protein Grb14

Rafael S. Depetris[1], **Junjie Hu**[1], **Ilana Gimpelevich**[1], **Lowenna J. Holt**[2], **Roger J. Daly**[2], and **Stevan R. Hubbard**[1,*]

[1]Structural Biology Program, Skirball Institute of Biomolecular Medicine and Department of Pharmacology, New York University School of Medicine, New York, New York 10016

[2]Cancer Research Program, Garvan Institute of Medical Research, Sydney, NSW 2010, Australia

Summary

Grb14, a member of the Grb7 adaptor protein family, possesses a pleckstrin homology (PH) domain, a C-terminal Src homology-2 (SH2) domain, and an intervening stretch of ~45 residues known as the BPS region, which is unique to this adaptor family. Previous studies have demonstrated that Grb14 is a tissue-specific negative regulator of insulin receptor signaling and that inhibition is mediated by the BPS region. We have determined the crystal structure of the Grb14 BPS region in complex with the tyrosine kinase domain of the insulin receptor. The structure reveals that the N-terminal portion of the BPS region binds as a pseudosubstrate inhibitor in the substrate peptide binding groove of the kinase. Together with the crystal structure of the SH2 domain, we present a model for the interaction of Grb14 with the insulin receptor, which indicates how Grb14 functions as a selective protein inhibitor of insulin signaling.

Introduction

Grb14 is a member of a family of adaptor proteins that also includes Grb7 and Grb10 (reviewed in Holt and Siddle [2005]). These proteins possess several signaling modules, including a Ras-associating domain, a PH domain, and a C-terminal SH2 domain, as well as polyproline sequences (Figure S1A available in the Supplemental Data with this article online). In addition, these proteins contain a ~45 residue region known as BPS (*b*etween *P*H and *S*H2) (He et al., 1998) or PIR (*p*hosphorylated *i*nsulin receptor-interacting *r*egion) (Kasus-Jacobi et al., 1998), which is unique to this adaptor family.

Grb7, Grb10, and Grb14 have been shown to be recruited to a variety of receptor tyrosine kinases (RTKs), including the insulin and insulin-like growth factor-1 (IGF1) receptors, ErbB2, platelet-derived growth factor receptor-β, Ret, EphB1, c-Kit, Tie2, and fibroblast

*Correspondence: hubbard@saturn.med.nyu.edu.

Supplemental Data

Supplemental Data include one figure and are available with this article online at http://www.molecule.org/cgi/content/full/20/2/325/DC1/.

Accession Numbers

Atomic coordinates have been deposited in the Protein Data Bank with ID codes as follows: Grb14(BPS)-IRK, 2AUH; Grb14(SH2), 2AUG.

growth factor receptor-1 (reviewed in Holt and Siddle [2005]). Recruitment of Grb7/10/14 to these activated (phosphorylated) RTKs is mediated by the phosphotyrosine binding SH2 domain and, for the insulin and IGF1 receptors exclusively, by the BPS region. Previous mutagenesis studies have indicated that both the SH2 domain and the BPS region target the phosphorylated activation loop in the tyrosine kinase domain of the insulin receptor (He et al., 1998).

Important insights into the biological role of Grb14 have come from a study of mice deficient for the Grb14 gene (Cooney et al., 2004). Male *Grb14*$^{-/-}$ mice exhibit improved glucose tolerance, despite lower circulating insulin levels, and enhanced insulin-induced signaling in muscle and liver, but not adipose tissue, demonstrating that Grb14 is a tissue-specific negative regulator of insulin signaling. There is also evidence that overexpression of Grb14 might contribute to insulin resistance (Cariou et al., 2004). In the *ob/ob* mouse model for non-insulin-dependent (type II) diabetes, Grb14 mRNA levels were found to be increased by 75%–100% in adipose tissue. In human type II diabetic patients, Grb14 mRNA levels were elevated by 43% in subcutaneous adipose tissue compared with nondiabetic control patients.

Previous biochemical studies have demonstrated that the BPS region of Grb7/10/14 is capable of directly inhibiting the catalytic activities of the insulin and IGF1 receptors (Stein et al., 2001; Bereziat et al., 2002), with a potency rank of Grb14 > Grb10 > Grb7 (Bereziat et al., 2002). Unlike the well-characterized architecture of the SH2 domain (reviewed in Kuriyan and Cowburn [1997]), the BPS region is unstructured, lacking secondary as well as tertiary structure (Moncoq et al., 2003).

To elucidate the molecular mechanism by which Grb14 negatively regulates signaling by the insulin receptor, we have determined the crystal structure of the Grb14 BPS region in complex with the phosphorylated kinase domain of the insulin receptor (IRK). The structure reveals the molecular basis for inhibition of IRK catalytic activity by the BPS region: the N-terminal portion of the BPS region binds as a pseudosubstrate inhibitor in the substrate peptide binding groove of the kinase.

Results

Crystal Structure of the Complex between the Grb14 BPS Region and IRK

Based on sequence similarity within the Grb7/10/14 family (Figure S1B), a protein encompassing the BPS region of Grb14 (Grb14[BPS]), residues 361–419, was used in cocrystallization trials with tris-phosphorylated IRK in which the activation-loop tyrosine residues (Tyr1158, Tyr1162, and Tyr1163) were phosphorylated. Crystals of a 1:1 Grb14(BPS)-IRK complex were obtained, and phasing from the IRK structure alone was sufficient to build residues 373–409 of Grb14(BPS). Although the structure has been refined at a modest resolution, 3.2 Å, the specific interactions between Grb14(BPS) and IRK are readily discernible, if not the precise interatomic distances. Data collection and refinement statistics are given in Table 1, and a $2F_o - F_c$ electron density map in the Grb14(BPS)-IRK interface region is shown in Figure 1D.

The crystal structure of the Grb14(BPS)-IRK complex reveals that the BPS region adopts several secondary structure features when bound to IRK, including two short β strands (β1 and β2) and a 16 residue-long C-terminal α helix (α1) (Figure 1A). The hallmark of the Grb14(BPS)-IRK structure is the positioning of the N-terminal portion of the BPS region in the substrate peptide binding groove of IRK. A superposition of the Grb14(BPS)-IRK structure with the structures of substrate peptides bound to IRK and to the IGF1 receptor kinase (Hubbard, 1997; Favelyukis et al., 2001) shows that the BPS-invariant sequence ^{376}LVAMDF binds as a pseudosubstrate, with the nonphosphorylatable Leu376 positioned in the kinase active site in place of a substrate tyrosine (Figure 1B).

IRK exhibits sequence specificity for tyrosine-containing substrates that possess hydrophobic residues at the +1 and +3 positions relative to the phosphorylatable tyrosine, particularly methionine at +3 (YXXM) (Shoelson et al., 1992; Zhou et al., 1995). The BPS pseudosubstrate region contains Val377 at the +1 position, Met379 at the +3 position, and Phe381 at the +5 position. These hydrophobic residues are virtually superimposable with Val(+1), Met(+3), and Phe(+5) from the IRS1-derived substrate peptides bound to IRK and the IGF1 receptor kinase (Figure 1B).

Optimal IRK substrates also possess acidic residues N-terminal to the substrate tyrosine (Zhou et al., 1995; Hubbard, 1997). The Grb14 BPS region contains a glutamic acid at the −3 position (Glu373), which in the crystal structure is salt bridged to Arg1089 of IRK (Figure 1C). Thus, from Glu373 to Phe381, the BPS region of Grb14 binds as an efficient substrate for IRK, save for Leu376 in the active site instead of a tyrosine.

After the pseudosubstrate region, the Grb14(BPS) polypeptide chain makes a turn, likely facilitated by BPS-conserved Gly383, and then folds back to interact with the pseudosubstrate region, forming, with the end of the IRK activation loop, a short three-stranded β sheet (Figure 1A). Two key residues in stabilizing the conformation of this portion of the BPS polypeptide are BPS-conserved Arg387 and Val388. Arg387 is salt bridged to Asp380, the +4 residue of the pseudosubstrate region, and to conserved Glu394 near the beginning of the BPS α helix (Figure 1C). Val388 makes van der Waals contacts with IRK residues in αG (Glu1216 and Leu1219) and with Val377 (+1) and Met379 (+3) of the BPS pseudosubstrate region.

The BPS α helix (α1) is initiated by conserved Asn391 and Pro392, the former of which is hydrogen bonded to the backbone amide nitrogen of Glu394 in an N-terminal helix-capping interaction (Figure 1C). The helix passes over the top of the IRK activation loop, and Val398, Glu402, and Trp406, which extend from the same face of the helix, make specific contacts with the loop (Figure 1D). The BPS-conserved Trp406 makes an unusual interaction with pTyr1163; the indole ring nitrogen is hydrogen bonded to the phosphate group (Figure 1D). pTyr1163, the third phosphotyrosine in the IRK activation loop, is the one most responsible for activation-loop stabilization (Hubbard, 1997). At its C-terminal end, α1 makes contacts with residues in αC in the N-terminal kinase lobe (Figure 1C). Van der Waals interactions are present between Gly403 and Arg1039, between Leu404 and Leu1038, and between Trp406 and Ile1042.

Crystal Structure of the Grb14 SH2 Domain

To gain further insights into the Grb14 interaction with IRK, we also determined the crystal structure of the Grb14 SH2 domain (Grb14[SH2]) at 2.3 Å resolution. The crystallographic statistics are given in Table 1. As expected from sequence identity (76%), the structure of Grb14(SH2) (Figure 2A) is very similar to the structure of Grb10(SH2) (Stein et al., 2003), with a root-mean-square deviation (rmsd) of 0.8 Å for 96 Cα atoms.

Besides an ordered DE segment, which extends the length of βD′ and βE (SH2 domain nomenclature according to Eck et al. [1993]), the only other notable difference between the Grb14(SH2) and Grb10(SH2) structures is the dimer interfaces. In the Grb14(SH2) structure, a noncrystallographic dimer is present, but it is distinct from the noncrystallographic Grb10(SH2) dimer. Intriguingly, in this Grb14(SH2) dimer, the phosphate binding pocket (containing conserved Arg466 [βB5]) of one protomer is completely occluded by the EF loop from the other protomer (and vice versa) (Figure 2B), indicating that formation of this dimer is incompatible with phosphotyrosine binding. In the Grb14(SH2) crystal structure, the Grb10(SH2)-like dimer is also present, but in the form of a crystallographic dimer, with Phe519 (αB8) in the center of the interface (Figure 2C). Gel filtration experiments on Grb14(SH2) mutants (data not shown) indicate that wild-type (wt) Grb14(SH2) is dimeric in solution and that the Phe519-mediated, Grb10(SH2)-like dimer is the predominant species. As in the Grb10(SH2) structure, a valine in the BG segment (Val526, BG3) instead of a glycine confers specificity for noncanonical, turn-containing phosphotyrosine sequences (Stein et al., 2003).

Biochemical Studies of the Interaction between Grb14 and the Insulin Receptor

To provide verification that the interaction between Grb14(BPS) and IRK as observed in the crystal structure occurs in a cellular context, we performed coimmunoprecipitation experiments with Chinese hamster ovary cells stably transfected with the insulin receptor (CHO-IR) and transiently transfected with full-length Grb14, either wt or mutant. We chose to mutate two BPS-conserved alanine residues to serine, a relatively conservative substitution. The first alanine, Ala378, is in the pseudosubstrate segment of BPS (+2 residue) and is close packed with residues from the BPS α helix. Mutation to a larger residue, even serine, would be predicted to disrupt binding of BPS to IRK. The second conserved alanine chosen for mutation, Ala399, is in the middle of the α helix, with space to accommodate a serine side chain. In addition, we substituted Trp406, which directly interacts with pTyr1163 in the activation loop (Figure 1D), with alanine. The coimmunoprecipitation results demonstrate that a serine substitution at Ala378 dramatically reduces Grb14 binding to the insulin receptor, as does the W406A mutation (Figure 3A). Also consistent with the structural predictions, the serine substitution at Ala399 causes little change in the interaction with the receptor.

The BPS region of Grb14 is a more potent inhibitor of insulin receptor catalytic activity than the BPS region of Grb7 or Grb10 (Bereziat et al., 2002). Of the 11 amino acid differences between Grb14 and Grb7 in the BPS region (Figure S1B), we made six individual Grb14→7, substitutions, which, judging from the crystal structure, were most likely to affect BPS binding to IRK. Coimmunoprecipitation experiments indicate that only one of the six

Grb14→7 substitutions, L404Q, had an appreciable effect on the interaction with the insulin receptor, which resulted in decreased binding (Figure 3B). Leu404 is near the C-terminal end of the BPS α helix and makes favorable hydrophobic contacts with the side chain of Leu1038 in αC (N-terminal kinase lobe) (Figure 1C).

To evaluate the contribution of the SH2 domain to the interaction between Grb14 and the insulin receptor, we mutated select SH2 domain residues and made a C-terminal deletion mutant that lacks the entire domain. Two mutants were made to target phosphotyrosine binding. The SH2-invariant Arg466 (βB5) was substituted with alanine (R466A), and a double lysine substitution, K484D (βD1) and K486A (βD3), was introduced. In the crystal structure of the SH2 domain of the adaptor protein APS bound to IRK (Hu et al., 2003), the equivalent arginine engages pTyr1158 in the activation loop and the equivalent lysines coordinate pTyr1162. A third amino acid substitution was introduced at Phe519, a key residue in SH2 domain dimerization (Figure 2C). As shown in Figure 3A, the R466A mutation dramatically decreased the interaction of Grb14 with the insulin receptor, to the level of the SH2 domain deletion. The K484D/K486A double mutation and the F519A mutation resulted in a several-fold loss of binding to the receptor. These biochemical studies indicate that high-affinity binding of Grb14 to the insulin receptor requires both the BPS region and a dimerized SH2 domain.

Grb14 Inhibition of Insulin-Stimulated Signaling

We tested in cells the ability of wt or mutant Grb14 to inhibit signaling events downstream of the insulin receptor. For this purpose, CHO-IR cells were transiently transfected with either wt Grb14 or the Grb14 mutants A378S and R466A, which disrupt binding to IRK of the BPS region and SH2 domain, respectively (Figure 3A). The phosphorylation levels of three signaling proteins downstream of the insulin receptor, IRS1, Akt, and ERK1/2, were determined by using phospho-specific antibodies to these proteins. Although the effects in this system were relatively modest, expression of wt Grb14 diminished the phosphorylation levels of all three proteins, with the effect on ERK1/2 being the most pronounced (Figure 3C, blots 1, 5, and 7). These results are generally consistent with those obtained in previous studies (Kasus-Jacobi et al., 1998; Bereziat et al., 2002). However, point mutations that disable either the SH2 domain (R466A) or, particularly, the BPS region (A378S) compromised the ability of Grb14 to suppress insulin signaling. Interestingly, the Grb14-mediated reduction in downstream phosphorylation occurred despite the higher phosphorylation level of the insulin receptor (Figure 3C, blot 3). Binding of Grb14 to the phosphorylated activation loop of the insulin receptor affords protection of these phosphotyrosines from protein tyrosine phosphatases such as PTP1B (Bereziat et al., 2002; Cooney et al., 2004).

Discussion

Mechanism and Specificity of Grb14 Inhibition of the Insulin Receptor

The crystal structure of Grb14(BPS)-IRK presented here provides the molecular basis for inhibition of the insulin receptor by Grb14: the BPS region binds as a pseudo-substrate in the substrate peptide binding groove of IRK and thus interferes with phosphorylation of

exogenous substrates (Figure 1B). The direct interaction of BPS residue Trp406 with pTyr1163 in the IRK activation loop (Figure 2D) nominally makes the BPS region a phosphotyrosine binding module. Yet this interaction is only one of many between Grb14(BPS) and IRK, all of which require the phosphorylation-stabilized configuration of the activation loop (Hubbard, 1997).

All three of the BPS-interaction regions on IRK—the substrate peptide binding groove, the activation loop, and αC—are highly characteristic of the insulin and IGF1 receptors, which explains the specificity of the BPS region of Grb7/10/14 for these two RTKs. Although 81% identical in sequence in the tyrosine kinase domain, the insulin receptor is inhibited by Grb14 to a greater extent (Bereziat et al., 2002). The residue composition of the substrate peptide binding groove of as is the activation loop. The difference in selectivity is possibly due to a sequence difference in αC. In the Grb14(BPS)-IRK structure, Leu1038 in αC makes van der Waals contacts with Leu404 in the BPS α helix (Figure 1C). In the IGF1 receptor, the Leu1038 equivalent is a methionine, which, because of its greater intrinsic flexibility, would provide a less favorable interaction with Leu404. Residue differences at the Leu404 position also explain why the BPS region of Grb14 is a more potent inhibitor of the insulin receptor than Grb7 (glutamine) (Figure 3B) and Grb10 (histidine).

Model of Grb14 Interaction with the Insulin Receptor

The SH2 domain is important for Grb14 binding to the insulin receptor (Figure 3A), and although not inhibitory to kinase activity by itself (Bereziat et al., 2002), it potentiates the inhibitory effect of the BPS region (Figure 3C). These data argue that the role of the SH2 domain is to increase binding affinity and to position the BPS region for interaction with the kinase domain. Our mutagenesis data (Figure 3A) support the hypothesis that the Grb14 SH2 domain engages the phosphorylated activation loop of IRK similarly to that of the APS SH2 domain (Hu et al., 2003).

A model for the interaction of the tandem BPS-SH2 region of Grb14 with the insulin receptor can thus be constructed, which is based on the crystal structures of Grb14(BPS)-IRK, Grb14(SH2), and APS(SH2)-IRK (Hu et al., 2003). In this model, pTyr1158, the first phosphotyrosine in the IRK activation loop, is bound in the canonical phosphate binding pocket of Grb14(SH2), coordinated by Arg466 (βB5), and pTyr1162 is coordinated by Lys484 (βD1) and Lys486 (βD3) (Figure 4A). All three of the activation-loop phosphotyrosines are thus engaged by Grb14: pTyr1158 and pTyr1162 by the SH2 domain and pTyr1163 by the BPS region (Trp406).

Dimerization of the Grb14 SH2 domain through its αB interface (Figure 2C) enhances the interaction of Grb14 with the insulin receptor (Figure 3A, F519A versus wt). A model of the dimerized BPS-SH2 region bound to the two tyrosine kinase domains of the insulin receptor β subunits (Figure 4B) is achieved by relating a second Grb14(BPS-SH2)-IRK complex to the first through the Grb14(SH2) dimer interface. In Grb14, the tether between the end of the PH domain, which presumably binds to phosphoinositides in the plasma membrane, and the beginning of the BPS region is relatively short, 16 residues, which will likely restrain the orientation of the SH2-dimerized kinase domains relative to the membrane (Figure 4B). In addition to direct inhibition of catalytic activity by Grb14, restraints on the spatial

positioning of the β subunits could limit access of downstream proteins such as IRS1/2 to the juxtamembrane recruitment site pTyr972.

Adaptor Proteins as Modulators of Insulin Signaling

Grb7, Grb10, and Grb14 exhibit similarities in domain organization to APS and SH2-B, two other adaptor proteins that bind to the activation loop of the insulin receptor via their SH2 domains (Kotani et al., 1998; Hu et al., 2003). All of these adaptors possess a central PH domain and an SH2 domain at or near the C terminus. In addition, they are dimeric (Stein et al., 2003; Hu et al., 2003; Nishi et al., 2005; this study), which facilitates their interaction with the two β subunits of the insulin receptor. Although the physiological roles of Grb7/10 and APS require further clarification, Grb14 functions as a negative modulator of insulin signaling (Bereziat et al., 2002; Cooney et al., 2004), whereas SH2-B is a positive modulator (Ahmed and Pillay, 2003; Duan et al., 2004). Our study highlights the mechanism by which the BPS region of Grb14, situated between the PH and SH2 domains, endows this adaptor protein with a negative insulin signaling function. Important questions that remain to be addressed are the spatial and temporal aspects of this regulatory mechanism and the interplay with protein tyrosine phosphatases.

Experimental Procedures

Protein Expression and Purification

IRK (residues 978–1283) was expressed in baculovirus-infected Sf9 insect cells, purified, and autophosphorylated in vitro as described previously (Hubbard, 1997). The cDNA encoding residues 361–419 of the human Grb14 BPS region was subcloned into the expression vector pGEX-4T-1 (Amersham Biosciences). The mutation C411S was introduced to avoid possible disulfide bond formation. The cDNA for the Grb14 SH2 domain (human, residues 433–537) was subcloned into pET14b (Novagen). pGEX-Grb14(BPS) and pET14b-Grb14(SH2) were transformed into *E. coli* strain BL21(DE3), and cultures were grown in Luria broth media at 37°C and induced with 1 mM isopropyl-thiogalactopyranoside (IPTG) at 30°C. Cells were harvested and resuspended in lysis buffer (50 mM Tris-HCl [pH 8.0], 300 mM NaCl, and complete protease inhibitor cocktail [Roche Diagnostics]) then lysed by French press and clarified by centrifugation. The GST-BPS fusion protein was isolated by GSTrap-affinity chromatography (Amersham Biosciences), cleaved by thrombin to remove GST, and further purified by Source-S (Amersham Biosciences) ion-exchange chromatography. The purified protein includes Grb14 residues 361–419 and two heterologous residues (GS) on the N terminus remaining from the thrombin cleavage site. Grb14(SH2) was purified by Ni-affinity (Qiagen) chromatography followed by Superdex-75 (Amersham Biosciences) gel filtration chromatography.

X-Ray Crystallography

Tris-phosphorylated IRK and Grb14(BPS) were mixed in a 1:2 molar ratio (as judged by OD_{280}) and concentrated to ~16 mg/ml. Crystals were grown at 4°C in hanging drops containing equal volumes of protein solution and reservoir buffer (15% [w/v] polyethylene glycol 8000, 100 mM sodium cacodylate [pH 6.5], and 50 mM calcium acetate). The crystals belong to hexagonal space group $P6_2$ with unit cell dimensions a = 127.18 Å, b =

127.18 Å, and c = 65.92 Å. There is one 1:1 complex in the asymmetric unit (solvent content of 67%). Before being flash frozen in liquid propane, crystals were transferred into a cryosolvent containing reservoir buffer plus 20% ethylene glycol. Data were collected on beamline X4A at the National Synchrotron Light Source and were processed by using DENZO/Scalepack (Otwinowski and Minor, 1997). A molecular replacement solution for IRK was found with AMoRe (Navaza, 1994) by using the structure of tris-phosphorylated IRK (PDB code 1IR3) (Hubbard, 1997) as a search model. Difference Fourier maps using phases calculated from the IRK model revealed appreciable electron density in the IRK active site and near the activation loop, attributable to the Grb14 BPS region. Multiple rounds of building and refinement of the BPS region were carried out with O (Jones et al., 1991) and CNS (Brünger et al., 1998). 12 residues (361–372) on the N terminus and ten residues on the C terminus (410–419) are disordered.

Crystals of Grb14(SH2) appeared in the stock protein solution (2 mg/ml in 50 mM HEPES [pH 7.5], 100 mM NaCl, and 1 mM DTT), on the sides of the microcentrifuge tube, after ~2 weeks at 4°C. MALDI-TOF mass spectrometry revealed that the crystals contained intact 6×His-Grb14(SH2). The crystals belong to trigonal space group $P3_121$ with two molecules per asymmetric unit and unit cell dimensions of a = b = 49.12 Å and c = 184.09 Å, giving a solvent content of 43.9%. The crystals were cryoprotected in the above buffer plus 20% ethylene glycol and then flash frozen in propane. Data were collected from a single crystal on a Rigaku RU-200 rotating anode equipped with an R-AXIS IIC image plate detector. A molecular replacement solution was obtained by using AMoRe, with the Grb10 SH2 domain (monomer; PDB code 1NRV) (Stein et al., 2003) as a search model.

Mammalian Cell Transfection, Immunoprecipitation, and Immunoblotting

The human Grb14 cDNA was cloned into the pRK5 vector containing an N-terminal Myc tag. Point mutations in Grb14 were generated by using QuikChange (Stratagene), and the mutations were confirmed by DNA sequencing. CHO-IR cells were maintained in α-minimal essential medium containing 10% fetal bovine serum plus antibiotics. The cells were transfected by Lipofectamine 2000 reagent (Invitrogen) for 6 hr. After 24 hr, the cells were serum deprived for 3 hr in Ham's F-12 medium. Cells were treated with insulin as indicated, washed twice with ice-cold phosphate-buffered saline, and lysed for 30 min at 4°C with buffer containing 50 mM Tris-HCl (pH 8.0), 135 mM NaCl, 1% Triton X-100, 1.0 mM EDTA, 1.0 mM sodium pyrophosphate, 1.0 mM sodium orthovanadate, 10 mM NaF, and protease inhibitors (Roche Diagnostics). For coimmunoprecipitation experiments, the clarified lysates were incubated with antibodies to Myc (Santa Cruz Biotechnology) for 1 hr at 4°C. The immune complexes were precipitated with protein A/G-aga-rose (Santa Cruz Biotechnology) for 1 hr at 4°C and were washed extensively with lysis buffer before solubilization in SDS-PAGE sample buffer. Bound proteins were resolved by SDS-PAGE and transferred to Immobilon-P polyvinylidene difluoride membranes (Millipore). Individual proteins were detected with the following antibodies: anti-insulin receptor β subunit (Santa Cruz Biotechnology or BD Transduction Laboratories); anti-insulin receptor pTyr1162/1163 and anti-IRS1 pTyr612 (BioSource International); anti-IRS1 (Upstate); anti-Akt, anti-Akt pSer473, anti-ERK1/2, and anti-phos-phoERK1/2 (Cell Signaling

Technology); and anti-Grb14 (Chemicon). Band visualization was performed by blotting with horse-radish peroxidase-conjugated secondary antibodies (BioSource International).

Supplementary Material

Refer to Web version on PubMed Central for supplementary material.

Acknowledgments

This work was supported by National Institutes of Health grant DK052916 (to S.R.H.) and grants from the National Health and Medical Research Council of Australia and Cancer Council New South Wales (to R.J.D). We thank N. Covino, G. Dorsainville, C. Scott, and E. Stein for experimental support; R. Ghirlando for sedimentation equilibrium studies; and R. Abramowitz and J. Wu for data collection assistance.

References

Ahmed Z, Pillay TS. Adapter protein with a pleckstrin homology (PH) and an Src homology 2 (SH2) domain (APS) and SH2-B enhance insulin-receptor autophosphorylation, extracellular-signal-regulated kinase and phosphoinositide 3-kinase-dependent signalling. Biochem J. 2003; 371:405–412. [PubMed: 12521378]

Bereziat V, Kasus-Jacobi A, Perdereau D, Cariou B, Girard J, Burnol AF. Inhibition of insulin receptor catalytic activity by the molecular adapter Grb14. J Biol Chem. 2002; 277:4845–4852. [PubMed: 11726652]

Brünger AT, Adams PD, Clore GM, DeLano WL, Gros P, Grosse-Kunstleve RW, Jiang JS, Kuszewski J, Nilges M, Pannu NS, et al. Crystallography & NMR system: A new software suite for macromolecular structure determination. Acta Crystallogr D Biol Crystallogr. 1998; 54:905–921. [PubMed: 9757107]

Cariou B, Capitaine N, Le Marcis V, Vega N, Bereziat V, Kergoat M, Laville M, Girard J, Vidal H, Burnol AF. Increased adipose tissue expression of Grb14 in several models of insulin resistance. FASEB J. 2004; 18:965–967. [PubMed: 15059968]

Cooney GJ, Lyons RJ, Crew AJ, Jensen TE, Molero JC, Mitchell CJ, Biden TJ, Ormandy CJ, James DE, Daly RJ. Improved glucose homeostasis and enhanced insulin signalling in Grb14-deficient mice. EMBO J. 2004; 23:582–593. [PubMed: 14749734]

Duan C, Yang H, White MF, Rui L. Disruption of the SH2-B gene causes age-dependent insulin resistance and glucose intolerance. Mol Cell Biol. 2004; 24:7435–7443. [PubMed: 15314154]

Eck MJ, Shoelson SE, Harrison SC. Recognition of a high-affinity phosphotyrosyl peptide by the Src homology-2 domain of p56lck. Nature. 1993; 362:87–91. [PubMed: 7680435]

Favelyukis S, Till JH, Hubbard SR, Miller WT. Structure and autoregulation of the insulin-like growth factor 1 receptor kinase. Nat Struct Biol. 2001; 8:1058–1063. [PubMed: 11694888]

He W, Rose DW, Olefsky JM, Gustafson TA. Grb10 interacts differentially with the insulin receptor, insulin-like growth factor I receptor, and epidermal growth factor receptor via the Grb10 Src homology 2 (SH2) domain and a second novel domain located between the pleckstrin homology and SH2 domains. J Biol Chem. 1998; 273:6860–6867. [PubMed: 9506989]

Holt LJ, Siddle K. Grb10 and Grb14: enigmatic regulators of insulin action — and more? Biochem J. 2005; 388:393–406. [PubMed: 15901248]

Hu J, Liu J, Ghirlando R, Saltiel AR, Hubbard SR. Structural basis for recruitment of the adaptor protein APS to the activated insulin receptor. Mol Cell. 2003; 12:1379–1389. [PubMed: 14690593]

Hubbard SR. Crystal structure of the activated insulin receptor tyrosine kinase in complex with peptide substrate and ATP analog. EMBO J. 1997; 16:5572–5581. [PubMed: 9312016]

Jones TA, Zou JY, Cowan SW, Kjeldgaard M. Improved methods for building protein models in electron density maps and the location of errors in these models. Acta Crystallogr A. 1991; 47:110–119. [PubMed: 2025413]

Kasus-Jacobi A, Perdereau D, Auzan C, Clauser E, Van Obberghen E, Mauvais-Jarvis F, Girard J, Burnol AF. Identification of the rat adapter Grb14 as an inhibitor of insulin actions. J Biol Chem. 1998; 273:26026–26035. [PubMed: 9748281]

Kotani K, Wilden P, Pillay TS. SH2-Balpha is an insulin-receptor adapter protein and substrate that interacts with the activation loop of the insulin-receptor kinase. Biochem J. 1998; 335:103–109. [PubMed: 9742218]

Kuriyan J, Cowburn D. Modular peptide recognition domains in eukaryotic signaling. Annu Rev Biophys Biomol Struct. 1997; 26:259–288. [PubMed: 9241420]

Moncoq K, Broutin I, Larue V, Perdereau D, Cailliau K, Browaeys-Poly E, Burnol AF, Ducruix A. The PIR domain of Grb14 is an intrinsically unstructured protein: implication in insulin signaling. FEBS Lett. 2003; 554:240–246. [PubMed: 14623073]

Navaza J. AMoRe: an automated package for molecular replacement. Acta Crystallogr A. 1994; 50:157–163.

Nishi M, Werner ED, Oh BC, Frantz JD, Dhe-Paganon S, Hansen L, Lee J, Shoelson SE. Kinase activation through dimerization by human SH2-B. Mol Cell Biol. 2005; 25:2607–2621. [PubMed: 15767667]

Otwinowski Z, Minor W. Processing of x-ray diffraction data collected in oscillation mode. Methods Enzymol. 1997; 276:307–326.

Shoelson SE, Chatterjee S, Chaudhuri M, White MF. YMXM motifs of IRS-1 define substrate specificity of the insulin receptor kinase. Proc Natl Acad Sci USA. 1992; 89:2027–2031. [PubMed: 1312712]

Stein EG, Gustafson TA, Hubbard SR. The BPS domain of Grb10 inhibits the catalytic activity of the insulin and IGF1 receptors. FEBS Lett. 2001; 493:106–111. [PubMed: 11287005]

Stein EG, Ghirlando R, Hubbard SR. Structural basis for dimerization of the Grb10 Src homology 2 domain. Implications for ligand specificity. J Biol Chem. 2003; 278:13257–13264. [PubMed: 12551896]

Zhou S, Carraway KL 3rd, Eck MJ, Harrison SC, Feldman RA, Mohammadi M, Schlessinger J, Hubbard SR, Smith DP, Eng C, et al. Catalytic specificity of protein-tyrosine kinases is critical for selective signalling. Nature. 1995; 373:536–539. [PubMed: 7845468]

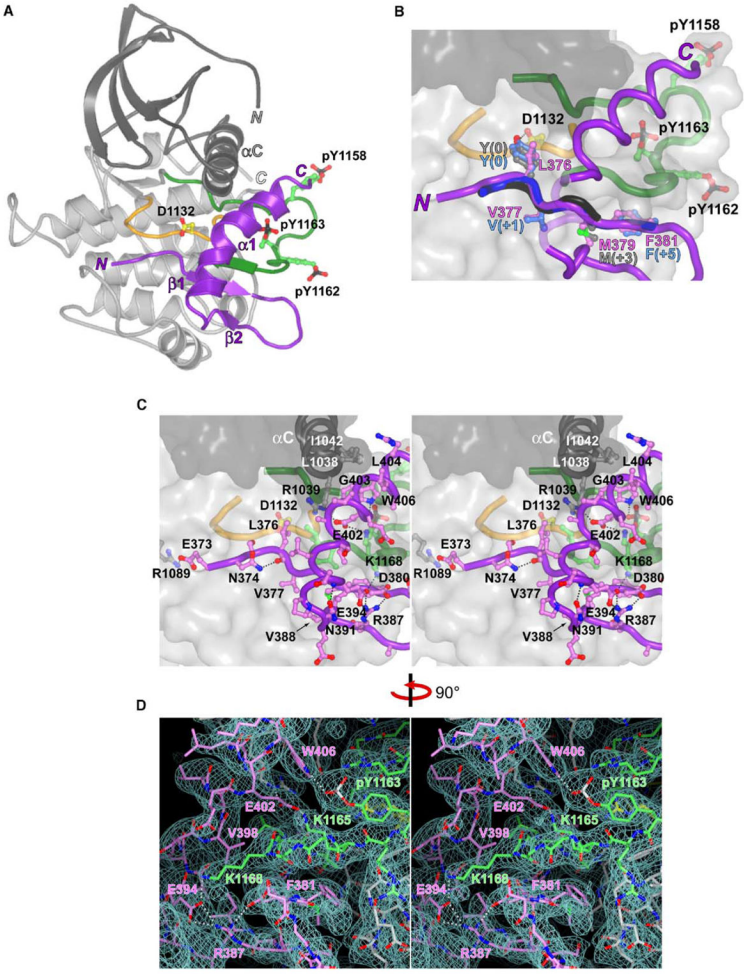

Figure 1. Crystal Structure of the Grb14(BPS)-IRK Complex

(A) Ribbon diagram of the complex between the Grb14 BPS region and phosphorylated IRK. The N-terminal lobe of IRK is colored dark gray, the C-terminal lobe is colored light gray, and Grb14(BPS) is colored purple. The catalytic loop of IRK (residues 1130–1137) is colored orange, and the activation loop (residues 1150–1171) is colored green. Select side chains in IRK are shown in ball-and-stick representation. Carbon atoms are colored yellow (in IRK catalytic loop) or green (in IRK activation loop), oxygen atoms are colored red, nitrogen atoms are colored blue, and phosphorus atoms are colored black. The N- and C termini of IRK and the BPS region are labeled (*N* and *C*) as are β1, β2, and α1 of BPS and αC in the N-terminal kinase lobe.

(B) View of the pseudosubstrate inhibitory region of Grb14(BPS). Superimposed on the Grb14(BPS)-IRK structure are IRS1-derived substrate peptides from the structures of peptide bound IRK (colored black) (Hubbard, 1997) and peptide bound IGF1 receptor kinase (colored blue) (Favelyukis et al., 2001). In addition to the substrate tyrosine Y(0), the side chains of residues in common with the BPS pseudosubstrate region are shown: Met(+3) of IRS1 ^{727}YMNM bound to IRK (colored gray) and Val(+1) and Phe(+5) of IRS1 ^{895}YVNIEF bound to the IGF1 receptor kinase (colored light blue). The dashed black

line represents a hydrogen bond between D1132 and the superimposed Y(0) from IRS1 ^{727}YMNM. A semitransparent surface is shown for IRK. The beginning of the BPS α helix is semitransparent to more easily view the pseudo-substrate region beneath. The viewing angle is the same as in (A).

(C) Stereo view of the interactions between Grb14(BPS) and IRK. All of the side chains of the BPS region are shown as well as select side chains of IRK. Hydrogen bonds/salt bridges are represented by dashed black lines. The coloring and viewing angle are the same as in (A).

(D) Stereo view of a $2F_o - F_c$ electron density map (3.2 Å, 1.0 σ contour) in the Grb14(BPS)-IRK interface. The viewing angle is 90° from that in (C), on the right. Carbon atoms are colored pink (BPS), green (IRK activation loop), yellow (IRK catalytic loop), or gray (rest of IRK), and phosphorus atoms are colored white. Hydrogen bonds/salt bridges are represented by dashed white lines. Figures 1, 2, and 4 were rendered with PyMOL software (http://pymol.sourceforge.net).

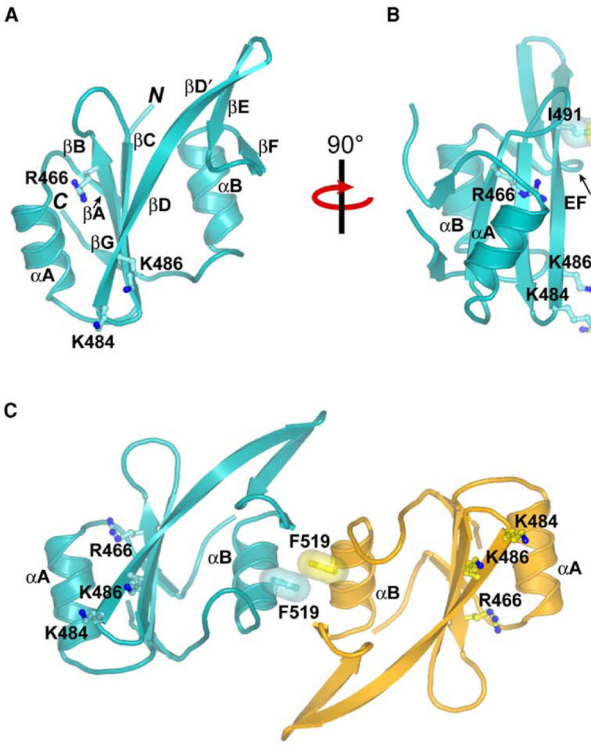

Figure 2. Crystal Structure of the Grb14 SH2 Domain

(A) Ribbon diagram of the Grb14 SH2 domain. The secondary structure elements are labeled. Shown in ball-and-stick representation are phosphotyrosine-interacting residues Arg466, Lys484, and Lys486.

(B) Ribbon diagram of the noncrystallographic Grb14 SH2 dimer. The two protomers are colored cyan and orange. The viewing angle is 90° from that in (A), as indicated. The noncrystallographic 2-fold axis is vertical, in the plane of the page. Ile491 in βD, shown with a van der Waals surface, is a key residue in this dimer interface.

(C) Ribbon diagram of the crystallographic Grb14 SH2 dimer. The crystallographic 2-fold axis is perpendicular to the page. The key residue in this dimer interface is Phe519 in αB, shown with a van der Waals surface.

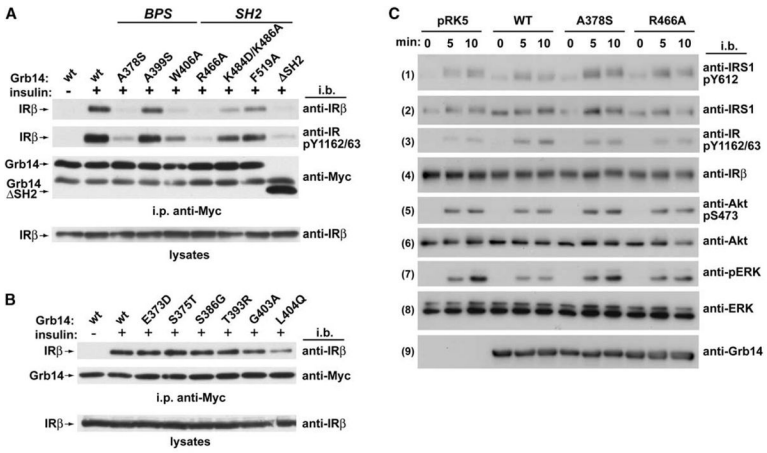

Figure 3. Interaction between Grb14 and the Insulin Receptor in Cells

(A) Myc-tagged Grb14 (wt or mutant) was transiently transfected into CHO-IR cells, and coimmunoprecipitations were performed after treatment with 20 nM insulin for 5 min. The lysates were immunoblotted with an antibody to the insulin receptor β subunit to confirm that approximately equal amounts of insulin receptor were present (bottom). Antibodies used for Western blotting are shown on the right side of the blots, and protein identification is supplied on the left side.

(B) Same as in (A), except the Grb14 mutations are to the equivalent residues in Grb7.

(C) CHO-IR cells were transiently transfected with plasmids coding for Myc-Grb14 (wt or mutant) or with empty vector pRK5, as indicated. Cells were stimulated with 1 nM insulin for 0, 5, or 10 min. Immunoblot analyses on the lysates were performed with the antibodies indicated on the right side of the blots. Blots 1, 3, 5, and 7, done with phospho-specific antibodies, show activation levels, and blots 2, 4, 6, 8, and 9 provide loading controls for the corresponding proteins.

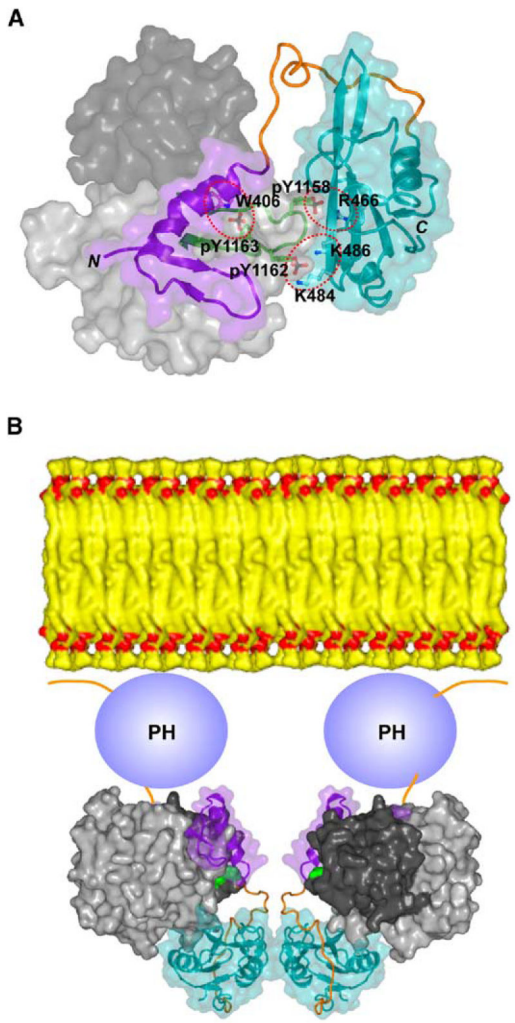

Figure 4. Model for the Interaction of Grb14 with the Insulin Receptor

(A) The interaction between the Grb14 SH2 domain and IRK is based on the APS(SH2)-IRK crystal structure (Hu et al., 2003). Coloring is the same as in Figure 1, with the SH2 domain colored cyan. Semitransparent surfaces are shown for IRK and for the BPS region and SH2 domain of Grb14. The 23 residue BPS-SH2 linker (colored orange) was modeled. The dashed red ovals highlight the interactions between Grb14 residues (labeled) and the activation-loop phosphotyrosines. The N terminus of the BPS region and the C terminus of the SH2 domain are labeled *N* and *C*, respectively.

(B) Model of the Grb14 dimer interacting with the two kinase domains of the insulin receptor β subunits. The dimeric form of the SH2 domain shown is the same as in Figure 2C. In this 2:2 complex, the N termini of the kinase domains (Tyr984, colored green) are 38 Å apart, with 32 residues of juxtamembrane region (not present in figure) linking each kinase domain to its transmembrane helix. The PH domain is shown schematically as interacting with the membrane. The N-terminal Ras-associating domain of Grb14 (see Figure S1A) is not depicted. The model is 2-fold symmetric about a vertical axis perpendicular to the plane

of a modeled membrane bilayer, which is colored yellow (carbon atoms) and red (oxygen atoms) and shown to scale.

Table 1

Data Collection and Refinement Statistics

	Grb14(BPS)-IRK	Grb14(SH2)
Data Collection		
Resolution (Å)	50–3.2	30–2.3
Observations (> 1σ)	39,467	57,590
Unique reflections	10,189	12,164
Redundancy	3.9	4.7
Completeness[a] (%)	99.8 (100.0)	99.7 (99.9)
R_{sym}[a,b] (%)	8.0 (37.7)	7.3 (16.6)
⟨I/σI⟩	14.3	14.2
Refinement[c]		
Resolution (Å)	30–3.2	30–2.3
Reflections	9,903	11,856
R_{cryst}[d]/R_{free} (%)	22.3/25.5	19.9/24.8
Rmsd bond lengths (Å)	0.008	0.005
Rmsd bond angles (°)	1.5	1.3
Rmsd B factors[e] (Å^2) (main/side chain)	1.2/1.5	0.9/1.2
Average B factors (Å^2)		
All atoms	44.8	16.5
SH2 domain	N/A	16.1
BPS region	44.9	N/A
IRK	44.6	N/A
Solvent	N/A	20.8

[a] Value in parentheses is for the highest resolution shell: 3.31–3.20 Å for Grb14(BPS)-IRK or 2.38–2.30 Å for Grb14(SH2).

[b] $R_{sym} = 100 - \Sigma|I - \langle I\rangle|/\Sigma I$.

[c] Atomic model for Grb14(BPS)-IRK: 2637 protein atoms and 2 Ca^{2+} ions (no water molecules). Atomic model for Grb14(SH2): 1745 protein atoms and 156 water molecules.

[d] $R_{cryst} = 100 \times \Sigma||F_O| \times |F_C||/\Sigma |F_O|$, where F_O and F_C are the observed and calculated structure factors, respectively ($F_O > 0\sigma$). R_{free} determined from 5% of the data.

[e] For bonded protein atoms.